JPNT 6(3), 105-116 (2017)
https://doi.org/10.11003/JPNT.2017.6.3.105

JPNT Journal of Positioning, Navigation, and Timing

Performance Analysis of the Wireless Localization Algorithms Using the IR-UWB Nodes with Non-Calibration Errors

Seong Yun Cho[1†], Dongyeop Kang[2], Jinhong Kim[2], Young Jae Lee[2], Ki Young Moon[2]

[1]Department of Robot Engineering, Kyungil University, Gyeongsan 38428, Korea
[2]Daegu-Gyeongbuk Research Center, Electronic and Telecommunications Research Institute, Daegu 42994, Korea

ABSTRACT

Several wireless localization algorithms are evaluated for the IR-UWB-based indoor location with the assumption that the ranging measurements contain the channelwise Non-Calibration Error (NCE). The localization algorithms can be divided into the Model-free Localization (MfL) methods and Model-based Kalman Filtering (MbKF). The algorithms covered in this paper include Iterative Least Squares (ILS), Direct Solution (DS), Difference of Squared Ranging Measurements (DSRM), and ILS-Common (ILS-C) methods for the MfL methods, and Extended Kalman Filter (EKF), EKF-Each Channel (EKF-EC), EKF-C, Cubature Kalman Filter (CKF), and CKF-C for the MbKF. Experimental results show that the DSRM method has better accuracy than the other MfL methods. Also, it demands smallest computation time. On the other hand, the EKF-C and CKF-C require some more computation time than the DSRM method. The accuracy of the EKF-C and CKF-C is, however, best among the 9 methods. When comparing the EKF-C and CKF-C, the CKF-C can be easily used. Finally, it is concluded that the CKF-C can be widely used because of its ease of use as well as it accuracy.

Keywords: IR-UWB, non-calibration error, model-free localization, model-based Kalman filtering, common bias

1. INTRODUCTION

The position information of humans, robots/transporters, and objects in an indoor space is required in diverse application fields. To resolve this issue, various methods have been studied and applied in practical life over the last decades (Kolodziej & Hjelm 2006). Research on pseudolite development and relevant technique was once a big issue, which was attributed to an aim of using an outdoor GPS receiver in an indoor space as it stands, but the commercialization was unsuccessful due to the problem of high-priced infrastructure installation (Kee et al. 2003). For localization that is not dependent on infrastructure, research on the Pedestrian Dead Reckoning (PDR) using inertial sensors has been performed for the last 20 years. With the performance improvement of MEMS-type inertial sensors, the method has become a solution that provides relatively stable position information. However, maintaining long-term accuracy is difficult when it is not combined with infrastructure, and the fact that the device needs to be installed on the body still serves as an obstacle to commercialization (Cho & Park 2006, Ju et al. 2015). The Wi-Fi Positioning System (WPS) techniques, which have been successfully commercialized by software development and the establishment of the database necessary for localization without investing a large sum of money in infrastructure installation, are based on the generalization of Wi-Fi Access Point (AP) installation and the popularization of a smartphone that includes a Wi-Fi transceiver module. The WPS techniques include: a method in which the database of the Media Access Control (MAC) address, which accords with the position information of installed AP, is established and localization is then performed based on trilateration and centroid techniques using the established database, and a method in which fingerprinting database is established and localization is then performed based on the K-Nearest Neighbor (KNN) algorithm using the established

Received Apr 21, 2017 **Revised** May 15, 2017 **Accepted** May 17, 2017
†**Corresponding Author**
E-mail: sycho@kiu.kr
Tel: +82-53-600-5584 Fax: +82-53-600-5599

fingerprinting database. The aforementioned techniques have recently been commercialized, and they have become popular techniques for indoor navigation. However, further research is required on the limitation of accuracy and the update of database (Cho & Park 2014, Cho 2016). When accurate position information is necessary, ultrasonic waves or Impulse Radio-Ultra Wideband (IR-UWB) can be used. In the case of ultrasonic waves, which are slower than radio waves traveling at the speed of light, accurate localization can be achieved on the strength of the small resolution of the measurable distance, but it cannot be used for wide-range localization due to the short coverage of its signal. Thus, ultrasonic waves are efficiently used for the robot localization in a small space. IR-UWB can provide a high-accuracy ranging solution with relatively wide coverage. In addition, the price of the transceiver chip has decreased in recent years, and the applicability has increased accordingly (Gezici et al. 2005, Oh et al. 2009).

In this study, the indoor localization technique using IR-UWB was investigated. IR-UWB is capable of accurate ranging based on the Two Way Ranging (TWR) or Symmetric Double Sided-TWR (SDS-TWR) techniques without any time synchronization. However, the distance measurement includes the environmental error, such as the multi-path error and Non-Line of Sight (NLOS) error, and the node internal error produced by the H/W and S/W of the transceiver (node) (Banani et al. 2013, Hur & Ahn 2014). The node internal error can be expressed as fixed errors for each channel, and it can be compensated through calibration before use. However, a user needs to perform calibration with background knowledge, and thus, the assumption that calibration is conducted before use in every application space may not be satisfied. In this study, therefore, it was assumed that the Non-Calibration Error (NCE) is basically included in the measurement.

The localization techniques using distance measurement can be classified into Model-Free Localization (MfL) and Model-based Kalman Filtering (MbKF). MfL is again classified into the iteration technique and the Linear Closed-form Solution (LCS) technique. The iteration technique includes the Iterative Least Squares (ILS) method, and the LCS technique includes the Direct Solution (DS) method and the Difference of Squared Ranging Measurements (DSRM) method (Park & Yim 2010, Cho & Kim 2013). MbKF is classified into the Constant Velocity (CV) model and the Constant Acceleration (CA) model according to the system model. As the measurement equation is nonlinear, it can also be classified into the Extended Kalman Filter (EKF), Unscented Kalman Filter (UKF), and Cubature Kalman Filter (CKF) according to the filter types. As mentioned above, there are various techniques for localization using distance measurement. These techniques have different characteristics, and show different performances depending on the measurement error characteristics. In this study, the characteristics of diverse localization algorithms were analyzed when NCE was included. For this purpose, an experiment was conducted, and the performances of the algorithms were analyzed based on the localization results when the same experiment data was applied to each algorithm.

The contents of this paper are as follows. In Chapter 2, IR-UWB-based ranging, ranging error, and the calibration technique are explained. In Chapter 3, various wireless localization algorithms are described; and in Chapter 4, the characteristics of each algorithm are analyzed based on the experimental results. The conclusions are summarized in the last chapter.

2. IR-UWB-BASED RANGING AND CALIBRATION

IR-UWB cannot measure the Time of Arrival (ToA) based on the time synchronization between nodes, and it calculates the distance by measuring the Round Trip of Flight (RToF) through TWR or SDS-TWR. When the distance between Node^A and Node^B is measured based on these two methods, the ranging errors can be expressed in Eq. (1), respectively.

$$\delta r_{TWR} = \frac{t_{reply\_B}(e^A - e^B)}{2} c$$
$$\delta r_{SDS-TWR} = \frac{(t_{reply\_A} - t_{reply\_B})(e^A - e^B)}{4} c \quad (1)$$

where t_{reply_i} is the time between the reception of the signal sent from another node and the retransmission of the signal in Node^i, and e^i is the clock error of Node^i. c is the travel speed of the signal, which is identical to the speed of light.

Based on Eq. (1), it can be found that SDS-TWR has superior performance compared to TWR. However, the clock error of each H/W is different although the same S/W is operated at the identically manufactured H/W. When the resultant time difference is multiplied by the speed of light, substantial ranging error could occur. Considering this, the ranging equation on a two-dimensional plane can be expressed by Eq. (2).

$$\tilde{r}^{A-B} = (1 + \delta SF^{A-B}) r^{A-B} + B^{A-B} + \delta^{A-B} + u^{A-B} \quad (2)$$

where r^{A-B} and $\tilde{r}^{A-B}$ are the actual distance and the measured

distance between Node^A and Node^B, respectively. $\delta SF^{A\text{-}B}$ and $B^{A\text{-}B}$ are the node internal errors due to NC, and they represent the scale factor error and the bias, respectively. $\delta^{A\text{-}B}$ is the ranging error due to environmental factors. $u^{A\text{-}B}$ is the noise, which is assumed to be white Gaussian.

In general, node internal error can be compensated through calibration. For this purpose, data are collected in a space where the Line of Sight (LOS) is guaranteed, while changing the distance between two nodes, and a parameter estimation algorithm is then carried out. In an LOS environment, when n measurements are obtained assuming that $\delta^{A\text{-}B}$ is absent in Eq. (2), it can be expressed by Eq. (3).

$$\begin{bmatrix} \tilde{r}_1^{A-B} - r_1^{A-B} \\ \vdots \\ \tilde{r}_n^{A-B} - r_n^{A-B} \end{bmatrix} = \begin{bmatrix} r_1^{A-B} & 1 \\ \vdots & \vdots \\ r_n^{A-B} & 1 \end{bmatrix} \begin{bmatrix} \delta SF^{A-B} \\ B^{A-B} \end{bmatrix} + \begin{bmatrix} u_1^{A-B} \\ \vdots \\ u_n^{A-B} \end{bmatrix} \quad (3)$$
$$\leftrightarrow \quad dR = HX + U$$

The scale factor error and the bias can be estimated based on the least squares method as shown in Eq. (4).

$$\begin{bmatrix} \delta\hat{S}F^{A-B} \\ \hat{B}^{A-B} \end{bmatrix} = (H^T H)^{-1} H^T dR \quad (4)$$

Using the estimated values, the distance measurement is compensated as shown in Eq. (5).

$$r^{A-B} \cong \frac{\tilde{r}^{A-B} - \hat{B}^{A-B}}{1 + \delta\hat{S}F^{A-B}} \quad (5)$$

When there are n nodes, this process needs to be carried out $n\,(n\text{-}1)/2$ times since it needs to be carried out based on every node pair. However, when this process is omitted, a large error could occur as the node internal error interacts with the environmental error factors.

3. WIRELESS LOCALIZATION ALGORITHMS

The localization error due to NC error could vary depending on the localization algorithms. In this chapter, various wireless localization algorithms are summarized, and the characteristics are analyzed. For this purpose, Eq. (2) is expressed as shown in Eq. (6).

$$\tilde{r}^{M-A} = (1 + \delta SF^{M-A})\sqrt{(x^A - x^M)^2 + (y^A - y^M)^2} + B^{M-A} + u^{M-A} \quad (6)$$

where the superscript M-A represents Mobile Node (MN)-Anchor Node (AN), and $A \in \{1, \ldots, n\}$.

The position of node on a two-dimensional plane could be expressed in the form of a complex number. In Eq. (6), ANs whose positions are accurately known were expressed as $\{p^A = x^A + jy^A\}_{A \in \{1, \ldots, n\}}$, and a MN whose position is to be estimated was expressed as $\{p^M = x^M + jy^M\}$.

3.1 ILS Method

For the ILS method, which is the most frequently used method for distance measurement-based wireless localization, Eq. (6) can be arranged as shown in Eq. (7), through the first-order expansion of the Taylor series.

$$\tilde{r}^{M-A} - r^{M-A^*} \cong r^{M-A^*}\delta SF^{M-A} + \frac{-(x^A - x^{M^*})}{r^{M-A^*}}\delta x^M + \frac{-(y^A - y^{M^*})}{r^{M-A^*}}\delta y^M + B^{M-A} + u^{M-A} \quad (7)$$

where $\{p^{M^*} = x^{M^*} + jy^{M^*}\}$ is the nominal point for the Taylor series expansion, and the calculated distance between AN^A and MN is expressed by $r^{M\text{-}A^*} = \sqrt{(x^A - x^{M^*})^2 + (y^A - y^{M^*})^2} = |p^A - p^M|$. $\{\delta p^M = \delta x^M + j\delta y^M\}$ is the error of the nominal point.

When the MN is connected with n ANs, the equation can be expressed as shown in Eq. (8) ignoring NCE (Mendel 1995).

$$\begin{bmatrix} \tilde{r}^{M-1} - r_k^{M-1^*} \\ \vdots \\ \tilde{r}^{M-n} - r_k^{M-n^*} \end{bmatrix} = \begin{bmatrix} \frac{-(x^1 - x_k^{M^*})}{r_k^{M-1^*}} & \frac{-(y^1 - y_k^{M^*})}{r_k^{M-1^*}} \\ \vdots & \vdots \\ \frac{-(x^n - x_k^{M^*})}{r_k^{M-n^*}} & \frac{-(y^n - y_k^{M^*})}{r_k^{M-n^*}} \end{bmatrix} \begin{bmatrix} \delta x_k^M \\ \delta y_k^M \end{bmatrix} + \begin{bmatrix} u^{M-1} \\ \vdots \\ u^{M-n} \end{bmatrix} \quad (8)$$

where the superscript M-j represents MN-AN j, and the subscript k represents the iteration sequence. Through the iteration, the position update and distance calculation are performed as shown in Eq. (9).

$$\{i_k^{M^*} = i_{k-1}^{M^*} + \delta\hat{i}_{k-1}^M\}_{i \in \{x, y\}} \quad (9a)$$

$$r_k^{M-A^*} = \sqrt{(x^A - x_k^{M^*})^2 + (y^A - y_k^{M^*})^2} \quad (9b)$$

When NCE is considered, it is not that every error for each channel can be estimated. It is because the measurement matrix cannot have a full rank. In this study, therefore, channel common bias was defined. Bias occurs during the process in which a signal is received at the antenna, is transmitted to RF chip, and is acquired by S/W; and thus it has a positive value at all times. In addition, when it is assumed that each node using the same H/W and S/W would have similar error characteristics, it is predicted that the bias for each channel would also have similar values. Therefore, the bias for each channel can be assumed to be common bias, and it can be included in the state variables to be estimated. In this regard, the scale factor has a value that

is relatively close to 0. When this value is included in the state variables and is to be estimated together, the connections between the MN and ANs are not sufficient, and accordingly, when the number of ranging data is less than 4, estimation cannot be performed as the measurement matrix cannot have a full rank. Therefore, in this study, the scale factor was not included in the state variables. As a result, it can be rearranged as shown in Eq. (10).

$$\begin{bmatrix} \tilde{r}^{M-1} - r_k^{M-1*} \\ \vdots \\ \tilde{r}^{M-n} - r_k^{M-n*} \end{bmatrix} = \begin{bmatrix} -\frac{x^1 - x_k^{M*}}{r_k^{M-1*}} & -\frac{y^1 - y_k^{M*}}{r_k^{M-1*}} & 1 \\ \vdots & \vdots & \vdots \\ -\frac{x^n - x_k^{M*}}{r_k^{M-n*}} & -\frac{y^n - y_k^{M*}}{r_k^{M-n*}} & 1 \end{bmatrix} \begin{bmatrix} \delta x_k^M \\ \delta y_k^M \\ B_k^{M-C} \end{bmatrix} + \begin{bmatrix} u^{M-1} \\ \vdots \\ u^{M-n} \end{bmatrix} \quad (10)$$

where B^{M-C} is the channel common bias. The position update is identical to that shown in (9a), and $r_k^{M-A^*}$ is calculated as shown in Eq. (11).

$$r_k^{M-A*} = \sqrt{(x^A - (x_{k-1}^{M*} + \delta\tilde{x}_{k-1}^M))^2 + (y^A - (y_{k-1}^{M*} + \delta\tilde{y}_{k-1}^M))^2} + \hat{B}_{k-}^M \quad (11)$$

In the ILS method, NCE can be considered, but error estimation for each channel is not possible, and channel common bias can be defined, estimated, and compensated. When the deviation of the bias for each channel is large, accurate error correction could be difficult, but the effectiveness will be analyzed through the experimental results in Chapter 4.

3.2 DS Method

The DS method is classified as the LCS technique among the MfL techniques, and the position solution can be expressed by Eq. (12).

$$\hat{p}_{DS}^M = L\left\{R_a + R_b\left(-b \pm \sqrt{|b^2 - 4ac|}\right)/2a\right\} \quad (12)$$

where each parameter can be found in Biton et al. (1998).

The DS method has a smaller computational load compared to the ILS method. However, there is a Red Sea Zone problem, where the error becomes large at the region in which the value of the square root in Eq. (12) is close to 0 depending on the position relationship among the ANs and MN (Cho & Kim 2013). In addition, this method expands the equation ignoring the scale factor error, bias, and measurement noise defined in Eq. (6); and thus the localization error due to NC becomes additionally larger.

3.3 DSRM Method

Among the LCS techniques, the DSRM method can be organized as shown in Eq. (13) considering the measurement noise.

$$\hat{p}_{DSRM}^M = (G^T Q^{-1} G)^{-1} G^T Q^{-1} Z \quad (13)$$

where G and Q can be found in (Cho & Kim 2013), and Z is expressed by Eq. (14).

$$Z = [\rho^{1-c} \quad \cdots \quad \rho^{(n-1)-c}]^T \quad (14)$$

where

$$\rho^{A-c} = \frac{(\tilde{r}^{M-A})^2 - (\tilde{r}^{M-C})^2 + (x^c)^2 + (y^c)^2 - (x^A)^2 - (y^A)^2}{2} \quad (15)$$

The important point of this method can be examined in $\{p^{A-c}\}_{A \in \{1, \ldots, (n-1)\}}$. When Eq. (6) is substituted into Eq. (15), it can be arranged as shown in Eq. (16) ignoring the multiplication of the errors.

$$\rho^{A-c} \cong \frac{(r^{M-A})^2 - (r^{M-C})^2 + (x^c)^2 + (y^c)^2 - (x^A)^2 - (y^A)^2}{2} + E^A + E^B + E^C + E^D \quad (16)$$

where

$$\begin{aligned} E^A &= (r^{M-A})^2 \delta SF^{M-A} - (r^{M-c})^2 \delta SF^{M-c} \\ E^B &= B^{M-A} u^{M-A} - B^{M-c} u^{M-c} \\ E^C &= r^{M-A} B^{M-A} - r^{M-c} B^{M-c} + \left\{(B^{M-A})^2 - (B^{M-c})^2\right\}/2 \\ E^D &= r^{M-A} u^{M-A} - r^{M-c} u^{M-c} + \left\{(u^{M-A})^2 - (u^{M-c})^2\right\}/2 \end{aligned} \quad (17)$$

Eq. (17) is included in the measurement error, and is analyzed as follows. The value of the scale factor error is close to 0, and thus E^A can be ignored. Assuming that the measurement noise is small and the bias is not large in the case of IR-UWB-based ranging, E^B also has a small value. The bias always has a positive value as explained in the previous section, and the bias for each channel is expected to show similar characteristics. Accordingly, E^C can be maintained at a small value, and a superior characteristic is expected in this regard, compared to the other methods. In addition, E^D is considered by Q in Eq. (13). In summary, the DSRM method is relatively less affected by NCE, compared to the other methods.

3.4 EKF

For the wireless localization using the Kalman filter, the state variables to be estimated and the dynamic model of a MN need to be selected by considering them together. In general, when the MN has a stable movement, a CV

model is selected, and the position and velocity are selected as the state variables. However, when the MN has a fast movement, a CA model is selected, and the position, velocity, and acceleration are selected as the state variables. In this study, a CV model was used, and a localization filter was designed using EKF since the measurement model is nonlinear as shown in Eq. (6). In the case of EKF, the error system model and the measurement model can be expressed by Eqs. (18) and (19) (Brown & Hwang 1997).

$$\begin{aligned}\delta X_{k+1} &= F\delta X_k + w_k,\ w_k \sim N(0,Q)\\ &= \begin{bmatrix}1 & T & 0 & 0\\ 0 & 1 & 0 & 0\\ 0 & 0 & 1 & T\\ 0 & 0 & 0 & 1\end{bmatrix}\begin{bmatrix}\delta x_k^M\\ \delta \dot{x}_k^M\\ \delta y_k^M\\ \delta \dot{y}_k^M\end{bmatrix} + w_k\end{aligned} \tag{18}$$

$$\begin{aligned}z_k &= H_k\delta X_k + v_k,\ v_k \sim N(0,R)\\ &= \begin{bmatrix}-\dfrac{x^1-\hat{x}_k^M}{\hat{r}_k^{M-1}} & 0 & -\dfrac{y^1-\hat{y}_k^M}{\hat{r}_k^{M-1}} & 0\\ \vdots & \vdots & \vdots & \vdots\\ -\dfrac{x^n-\hat{x}_k^M}{\hat{r}_k^{M-n}} & 0 & -\dfrac{y^n-\hat{y}_k^M}{\hat{r}_k^{M-n}} & 0\end{bmatrix}\begin{bmatrix}\delta x_k^M\\ \delta \dot{x}_k^M\\ \delta y_k^M\\ \delta \dot{y}_k^M\end{bmatrix} + v_k\end{aligned} \tag{19}$$

where $\{\delta v^M = \delta \dot{x}^M + j\delta \dot{y}^M\}$ is the velocity error of the MN, and T is the time propagation period of the filter, which is identical to the distance measurement acquisition period. Q and R are the processor noise covariance matrix and the measurement noise covariance matrix, respectively.

The position of the MN is updated as shown in Eq. (20) at the frequency of ranging, and it is then compensated as shown in Eq. (21) using the error estimates.

$$p_k^{M-} = p_{k-1}^M + v_{k-1}^M \cdot T \tag{20}$$

$$p_k^M = p_k^{M-} + \delta \hat{x}_k^M + j\delta \hat{y}_k^M \tag{21}$$

where the superscript - represents the time propagation.

When there is NCE, it can be added as a state variable. In the filter, only the bias is estimated excluding the scale factor error. When all the biases for each channel are added, the error state variable and the system and measurement matrices are designed as shown in Eq. (22-24).

$$\delta X_k = \begin{bmatrix}\delta x_k^M & \delta \dot{x}_k^M & \delta y_k^M & \delta \dot{y}_k^M & \delta B_k^{M-1} & \cdots & \delta B_k^{M-n}\end{bmatrix}^T \tag{22}$$

$$F = \begin{bmatrix}\overline{F} & 0_{4\times N}\\ 0_{N\times 4} & I_{N\times N}\end{bmatrix} \tag{23}$$

$$H_k = \begin{bmatrix}\overline{H}_k & h\end{bmatrix} \tag{24}$$

where $\overline{F}$ and $\overline{H}_k$ are the system matrix and the measurement matrix used in Eqs. (18) and (19), respectively. $h = I_{n\times N}$, and N represent the number of measurements (n). The distance calculation is $\hat{r}^{M\text{-}A} = \sqrt{(x^A - \hat{x}_k^{M-})^2 + (y^A - \hat{y}_k^{M-})^2} + \hat{B}_{k-1}^{M\text{-}A} \cdot \delta\hat{B}_k^{M\text{-}A}$ in the state variables is the bias estimation error of Channel A.

The filter operation is identical to that shown in Eqs. (20-21), and only the bias estimation update is added as shown in Eq. (25).

$$\hat{B}_k^{M-A} = \hat{B}_{k-1}^{M-A} + \delta\hat{B}_k^{M-A} \tag{25}$$

In this case, the observability for the estimation of each bias needs to be analyzed, and it will be analyzed through the test results in Chapter 4. If the degree of observability is low, the accuracy of the estimated bias can be low. Considering this, the design can be implemented using channel common bias, similar to the design of the ILS method. In that case, the error state variable is expressed by Eq. (26).

$$\delta X_k = \begin{bmatrix}\delta x_k^M & \delta \dot{x}_k^M & \delta y_k^M & \delta \dot{y}_k^M & \delta B_k^{M-C}\end{bmatrix}^T \tag{26}$$

In the case of the system matrix, N is set to 1 in Eq. (23); and in the case of the measurement matrix, $h = [1 \ldots 1]^T$ in Eq. (24). The distance calculation is $\hat{r}_k^{M\text{-}A} = \sqrt{(x^A - \hat{x}_k^{M-})^2 + (y^A - \hat{y}_k^{M-})^2} + \hat{B}_{k-1}^{M\text{-}C}$.

3.5 CKF

To analyze the localization characteristics depending on the type of the filter, a localization filter was designed using CKF. CKF is an approximate Bayesian filter based on the cubature rule, and it is known that the characteristics of the third-order CKF are similar to those of UKF. For the model, a CV model was used, similar to EKF. When the NCE model is not considered, the number of state variables is 4, and thus eight Cubature Points (CP) are established (Arasaratnam & Haykin 2009). When the distance measurement is obtained, time propagation is performed as shown in Eq. (27).

$$\left\{\begin{aligned}\hat{\xi}_k^-(i,1) &= \hat{\xi}_{k-1}(i,1) + \hat{\xi}_{k-1}(i,2)\cdot T\\ \hat{\xi}_k^-(i,3) &= \hat{\xi}_{k-1}(i,3) + \hat{\xi}_{k-1}(i,4)\cdot T\end{aligned}\right\}_{i=1,2,\cdots,2N} \tag{27}$$

where ξ is the matrix that defines CP, and the subscripts in parentheses (i, j) represent the i-th row and the j-th column. The columns of each row represent the x-axis position, the x-axis velocity, the y-axis position, and the y-axis velocity, respectively. N is the order of the state variable, which is 4.

After the time propagation of CP, the state variable ($\hat{x}_k^-$) and the error covariance matrix (P_k^-) are calculated. The measurement update is then carried out as shown in Eqs. (28) and (29).

$$\hat{x}_k = \hat{x}_k^- + P_{xz,k}(P_{zz,k} + R)^{-1}\left([\tilde{r}_k^{M-1} \quad \cdots \quad \tilde{r}_k^{M-n}]^T - \hat{z}_k^-\right) \quad (28)$$

$$P_k = P_k^- - P_{xz,k}(P_{zz,k} + R)^{-1}P_{xz}^T \quad (29)$$

where P_{xz} and P_{zz} are the cross-covariance martix of the state variable and the measurement, and the measurement covariance matrix, respectively. The measurement is calculated as shown in Eq. (30).

$$\hat{z}_k^- = \sum_{i=1}^{2N} \frac{1}{2N}[\hat{r}_k^{M-1}(i) \quad \cdots \quad \hat{r}_k^{M-n}(i)]^T$$

$$\hat{r}_k^{M-A}(i) = \sqrt{(x^A - \hat{\xi}_k^-(i,1))^2 + (y^A - \hat{\xi}_k^-(i,3))^2} \quad (30)$$

CP is then updated.

The CKF-based localization filter can also be designed considering NCE, similar to EKF. In this study, the design was implemented using only the channel common bias, and the number of state variables is $N = 4 + 1$. The measurement is generated as shown in Eq. (31).

$$\hat{r}_k^{M-A}(i) = \sqrt{(x^A - \hat{\xi}_k^-(i,1))^2 + (y^A - \hat{\xi}_k^-(i,3))^2} + \hat{\xi}_k^-(i,5) \quad (31)$$

where $\hat{\xi}_k^-(i, 5)$ is the CP that corresponds to the channel common bias.

In the case of CKF, it is unnecessary to obtain the Jacobian matrix, which is calculated by the first-order Taylor series expansion of a nonlinear function, and only the relational expression needs to be accurately described using each CP for the measurement generation. Accordingly, the filter design can be easily carried out.

4. ANALYSIS OF THE ALGORITHM CHARACTERISTICS BASED ON THE EXPERIMENTAL RESULTS

To compare and analyze the performances of the various localization algorithms explained in Chapter 3, some experiments were conducted. For the IR-UWB equipment, four EVK1000 devices (Decawave) shown in Fig. 1 were used. Among them, three devices were used as ANs, and one device was used as a MN. According to the specification provided by Decawave, it is capable of communication up to 290 m with a ranging precision of 10 cm.

4.1 Calibration Test

To examine the NCE of the used equipment, three ANs were installed and ten reference points were established in an environment where LOS is guaranteed, as shown in Fig. 2. Then, a MN was located at each reference point, and the ranging information was obtained through communication

Fig. 1. IR-UWB module: EVK1000 (Decawave).

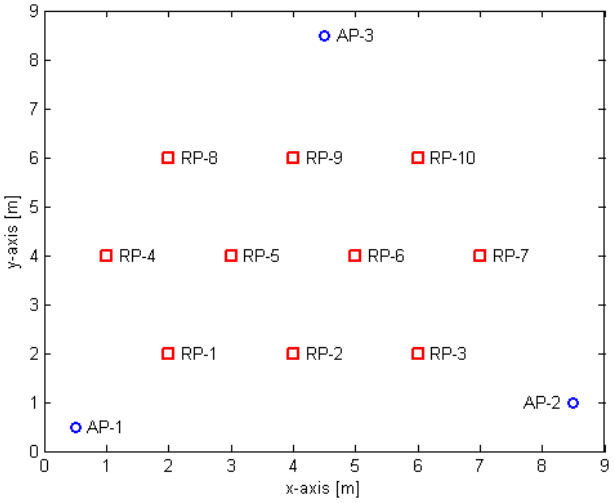

Fig. 2. Calibration test environment.

with the ANs during a certain time.

Table 1 summarizes the scale factor error and bias for each channel estimated based on Eq. (4). For the scale factor error, the values were small in general, although M-3 had a relatively large value. In the case of the bias, all the values were positive. As for the establishment of channel common bias, there was some difference between channels, but the error setting and estimation results will be analyzed in the algorithm test.

Table 1 and Fig. 3 show the ranging results before and after the calibration. An average of about 70 ranging measurements were obtained on ten reference points,, and the analysis result showed that the average error was 29 cm with a standard deviation of 10 cm before the calibration. In other words, this indicates that the calibration of the product on the market was not properly conducted. For the ranging error after the calibration, the standard deviation was similar to that before the calibration, but the average value decreased significantly.

Table 1. Channel-wise calibration results.

Channel [m]	$\delta\hat{S}F^{Channel}$	$\hat{B}^{Channel}$	Ranging error before calibration		Ranging error after calibration	
			Mean	Standard deviation	Mean	Standard deviation
M-1	0.00744	0.25933	0.21841	0.11376	-5.4e-14	0.11301
M-2	0.00829	0.39504	0.34629	0.10387	-4.4e-14	0.10288
M-3	0.05141	0.57882	0.30556	0.10208	4.9e-14	0.07336

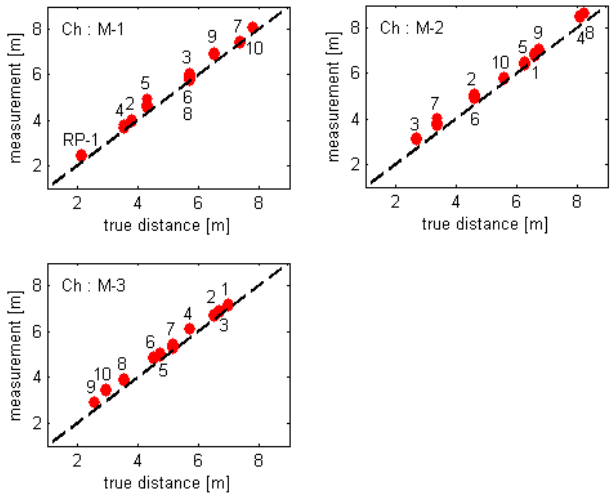

(a)

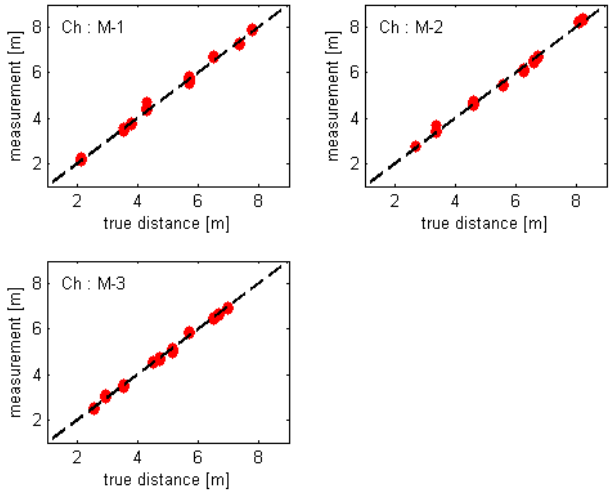

(b)

Fig. 3. Ranging results before/after calibration. (a) before calibration (b) after calibration.

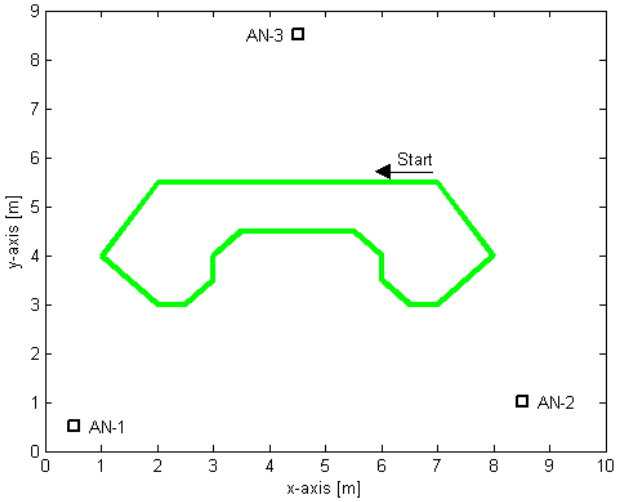

Fig. 4. Test trajectory for evaluating the localization algorithms.

4.2 Localization Algorithm Test

A test was conducted to analyze the performances of the various localization algorithms explained in Chapter 3 in the presence of NCE. Fig. 4 shows the test trajectory. A test participant carried a MN, and walked along the trajectory. Nine algorithms were used: ILS, DS, DSRM, ILS-C, EKF, EKF-EC, EKF-C, CKF, and CKF-C. In this regard, Each Channel (EC) indicates that the biases for each channel were augmented as the state variable, and Common (C) indicates that the channel common bias was augmented as the state variable. As three ANs were used, 7th-order filter is operated in the case of EC, and 5th-order filter is operated in the case of C. Based on the repeated tests, similar results were obtained for each algorithm. Among these, one test result was shown in Fig. 5. Figs. 5a-i show the localization results for the nine algorithms (from ILS to CKF-C). Fig. 5j shows the estimated bias for each channel of EKF-EC, Fig. 5k shows the estimated common bias for ILS-C, EKF-C, and CKF-C, respectively, and Fig. 5l shows the square root of the estimation error covariance of the state variable corresponding to the bias for EKF-EC and EKF-C, respectively. In Figs. 5a, b, c, e, and h, the blue circle marker represents the case in which NCE was present, and the red triangular marker represents the case in which the localization was performed after the calibration. For the test, there was no reference equipment that can represent the accurate position of a MN. Thus, the localization accuracy was judged by comparing the estimated position with the walking trajectory.

Basically, better results were obtained after the calibration than before the calibration. However, there are two noteworthy points. First, in the case of the DS method, a large estimation error was observed in a specific region regardless of the calibration. This is because the Red Sea Zone problem occurred in the corresponding region (Cho & Kim 2013). Second, in the case of the DSRM method, the result before

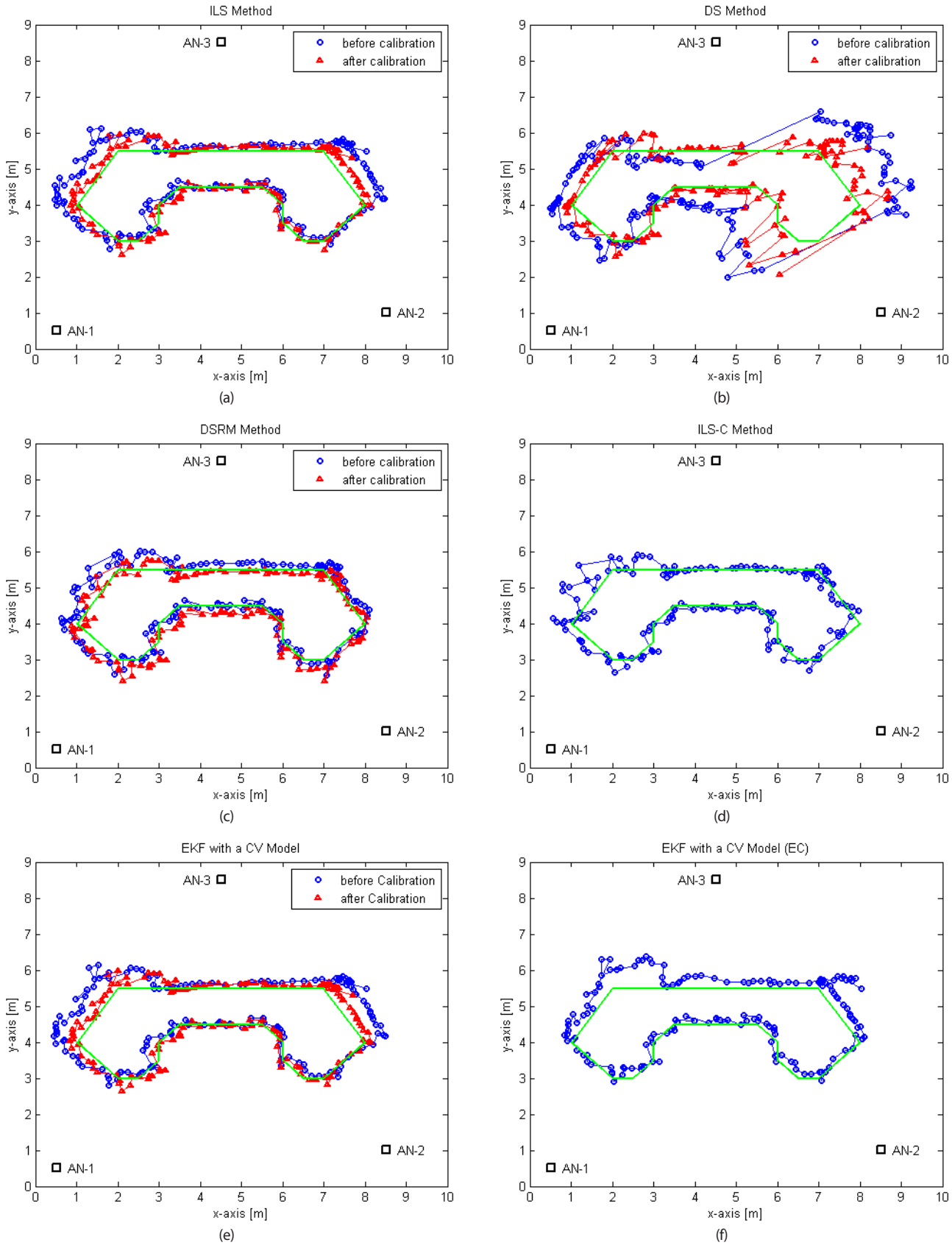

Fig. 5. Results of the localization tests according to the algorithms. (a) ILS method (b) DS method (c) DSRM method (d) ILS-C method (e) EKF (f) EKF-EC (g) EKF-C (h) CKF (i) CKF-C (j) channel-wise bias estimates (k) common bias estimates (l) error covariance

https://doi.org/10.11003/JPNT.2017.6.3.105

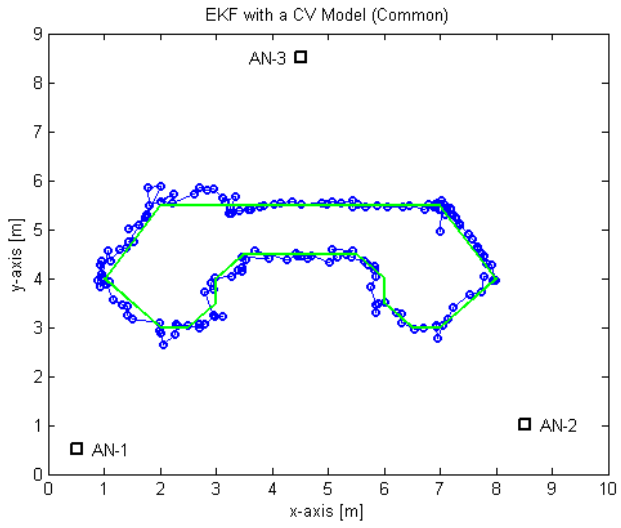

(g)

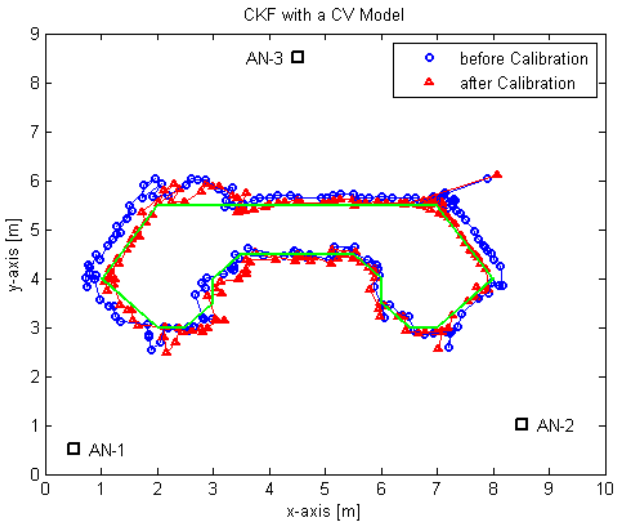

(h)

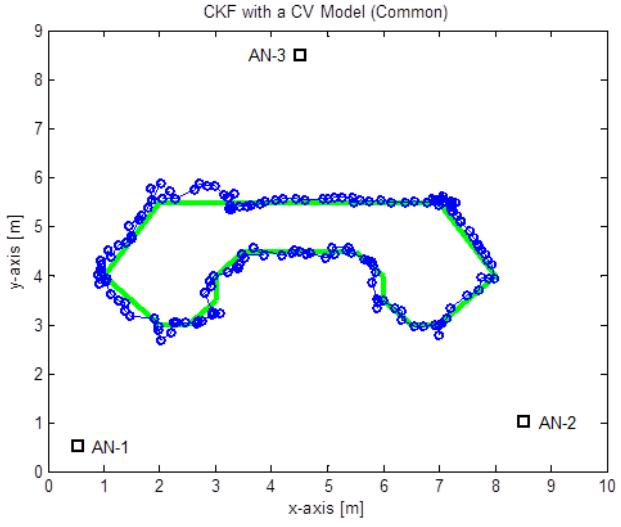

(i)

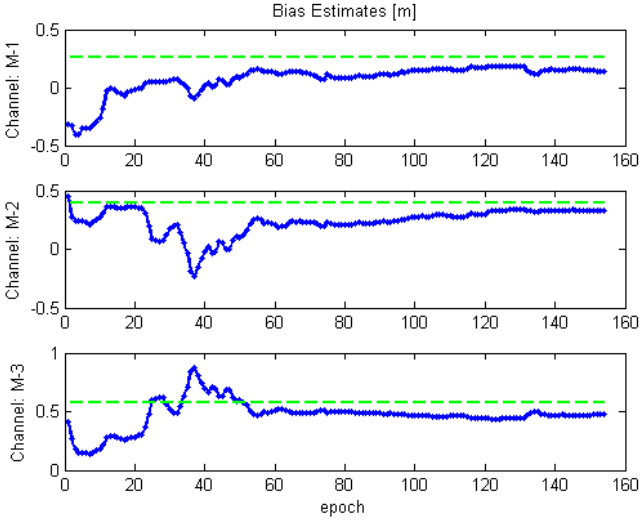

(j)

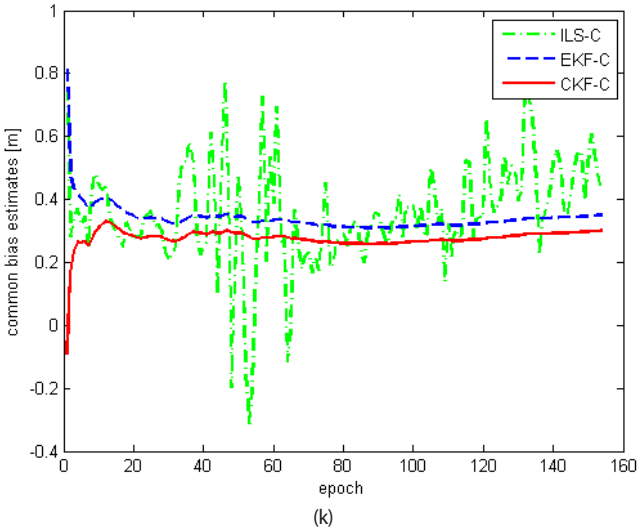

(k)

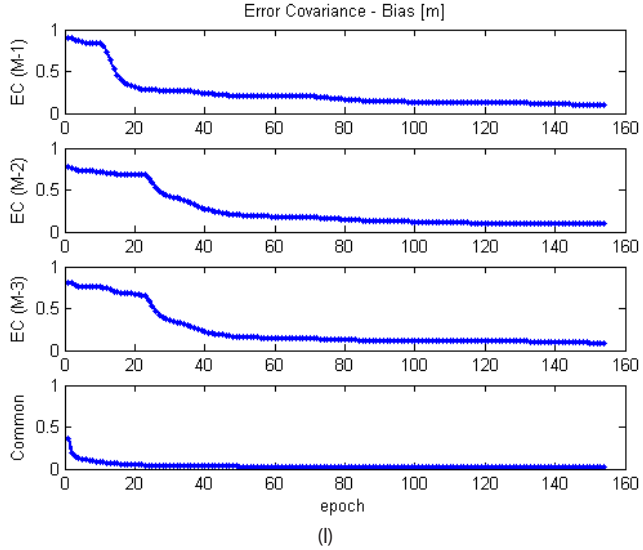

(l)

Fig. 5. *Continued*

the calibration was more outstanding, compared to the other methods. This is because the error included in the ranging measurement was partially eliminated in the process of subtracting the square of the ranging measurement for the DSRM method, as explained in Section 3.3. Therefore, the DSRM technique could show more outstanding characteristics in the presence of NCE, compared to the other methods.

Based on Figs. 5f, j, and l, the performance of the bias estimation for each channel was analyzed. As shown in Fig. 5j, the biases for the three channels were gradually approximately estimated. However, the convergence rate was not fast. The analysis based on Fig. 5l indicates that this is because the decrease rate of the estimation error covariance of the state variable corresponding to the bias for each channel was slow. Accordingly, a large error was observed on the upper left part of the walking trajectory, which is before the convergence of the estimation error.

In comparison, the estimation performance of the case in which common bias was added to the state variable was analyzed based on Figs. 5d, g, i, k, and l. Figs. 5d and k show the result where common bias was added and estimated together in ILS-C, as explained in Section 3.1. The comparison with EKF-C and CKF-C in Fig. 5k indicated that similar common bias was estimated. In ILS-C, however, the bias is independently estimated for each measurement, and thus it does not have convergence characteristics depending on the time. As a result, the bias was partially estimated and compensated on the walking trajectory. When compared to the results of the MfL methods before the calibration excluding the DSRM method, relatively outstanding performance was observed. On the other hand, Figs. 5g and i show the localization results where the common bias was estimated in EKF-C and CKF-C, respectively. The results were similar to those of the ILS, DSRM, and EKF with the calibration. As for the reason analyzed based on Figs. 5k and l, they showed more outstanding characteristics than EKF-EC because the estimation speed of the state variable corresponding to the common bias was fast. Also, they showed more outstanding characteristics than ILS-C because the common bias estimate converged as the measurement update was carried out since the measurement used for the estimation at each epoch has the characteristics of an infinite impulse response filter which uses all the previous measurements together.

Fig. 6 shows the average computation time for each epoch obtained through the tic/toc commands of Matlab. CKF has a relatively large computational load as it performs the time propagations of CPs that correspond to twice the dimension of the system. ILS also has a large computational load as the

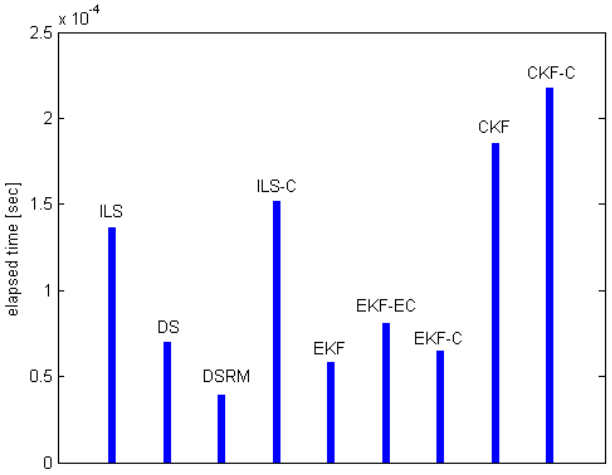

Fig. 6. Elapsed times of the localization algorithms.

calculation is based on iterative processing. On the other hand, in the case of DSRM, the number of measurements decreases by 1 through measurement differencing, in terms of the calculation.

Based on the results of this study, the following conclusions can be drawn. Localization error occurs when calibration is not performed in the presence of NCE, and this error can be compensated through the bias estimation for each channel or the common bias estimation. The results indicated that the methods using the common bias estimation showed more outstanding performance than the methods using the bias estimation for each channel. This is because every bias for each channel had a positive value and the difference between channels was not large. The DSRM technique was found to have relatively outstanding characteristics as it was less affected by NCE despite the shortest computation time compared to the other methods. EKF-C and CKF-C showed the most outstanding performances although the computational load was large. In particular, considering the ease of filter design, CKF-C was easier to use than EKF-C.

5. CONCLUSIONS

In this study, the performances of the various algorithms for the wireless localization using IR-UWB-based ranging measurement were compared and analyzed. In particular, when NCE was included in the ranging measurement, the localization characteristics of nine algorithms (ILS, DS, DSRM, ILS-C, EKF, EKF-EC, EKF-C, CKF, and CKF-C) were first analyzed based on the algorithm equation expansion process, and conclusions were drawn based on the results of an experiment.

The analysis of the experiment indicated that the NCE

for each channel had a positive value at all times, and the difference between channels was not large. In this case, among the MfL methods, the DSRM method showed outstanding localization characteristics although the error for each channel was not considered. In the case of MbKF, when the biases for each channel were augmented to the state variable, improved results could not be obtained as the estimation speed was slow. However, when common bias was augmented to the state variable and was estimated/compensated, the bias estimation speed was fast, and accordingly, the localization performance was relatively outstanding.

CKF-C had the longest computation time, and the DSRM method had the shortest computation time. Therefore, the DSRM method showed outstanding characteristics when the computation time and the localization performance were considered, and CKF-C showed relatively outstanding characteristics when the accuracy and the ease of filter design were considered.

ACKNOWLEDGMENT

This research was partially supported by Basic Science Research Program through the National Research Foundation of Korea (NRF) funded by the Ministry of Education (NRF-2015R1D1A1A01059606).

This work was partially supported by the ICT R&D program of IITP. [R7119-16-1014, Development of the smart AEO automation platform based on the standard IoT platform for import and export SMEs]

REFERENCES

Arasaratnam, I. & Haykin, S. 2009, Cubature Kalman filters, IEEE Trans. Automatic Control, 54, 1254-1269. https://doi.org/10.1109/TAC.2009.2019800

Banani, S. A., Najibi, M., & Vaughan, R. G. 2013, Range-based localisation and tracking in non-line-of-sight wireless channels with Gaussian scatterer distribution model, IET Communications, 7, 2034-2043. https://doi.org/10.1049/iet-com.2012.0265

Biton, I., Koifman, M., & Bar-Itzhack, I. Y. 1998, Improved direct solution of the global positioning system equation, Journal of Guidance, Control and Dynamics, 21, 45-49. https://doi.org/10.2514/2.4195

Brown, R. G. & Hwang, P. Y. C. 1997, Introduction to Random Signals and Applied Kalman Filtering (New York: John Wiley & Sons)

Cho, S. Y. 2016, Measurement error observer-based IMM filtering for mobile node localization using WLAN RSSI measurement, IEEE Sensors Journal, 16, 2489-2499. https://doi.org/10.1109/JSEN.2015.2512590

Cho, S. Y. & Kim, B. D. 2013, Linear closed-form solution for wireless localisation with ultra-wideband/chirp spread spectrum signals based on difference of squared range measurements, IET-Wireless Sensor Systems, 3, 255-265. https://doi.org/10.1049/iet-wss.2012.0159

Cho, S. Y. & Park, C. G. 2006, MEMS based pedestrian navigation system, Journal of Navigation, 59, 135-153. https://doi.org/10.1017/S0373463305003486

Cho, S. Y. & Park, J. G. 2014, Radio propagation model and spatial correlation method-based efficient database construction for positioning fingerprints, Journal of Institute of Control, Robotics and Systems, 20, 774-781. https://doi.org/10.5302/J.ICROS.2014.14.0010

Gezici, S, Tian, Z, Giannakis, G. B., Kobayashi, H., Molisch, A. F., et al. 2005, Localization via ultra-wideband radio: a look at positioning aspects for future sensor networks, IEEE Signal Processing Magazine, 22, 70-84. https://doi.org/10.1109/MSP.2005.1458289

Hur, H. & Ahn, H.-S. 2014, Unknown input observer-based filtering for mobile pedestrian localization using wireless sensor networks, IEEE Sensors Journal, 14, 2590-2600. https://doi.org/10.1109/JSEN.2014.2312193

Ju, H., Lee, M. S., Park, S. Y., Song, J. W., & Park, C. G. 2015, A pedestrian dead-reckoning system that considers the heel-strike and toe-off phases when using a foot-mounted IMU, Measurement Science and Technology, 27, 015702. https://doi.org/10.1088/0957-0233/27/1/015702

Kee, C., Jun, H., & Yun, D. 2003, Indoor navigation system using asynchronous pseudolites, Journal of Navigation, 56, 443-455. https://doi.org/10.1017/S0373463303002467

Kolodziej, K. W. & Hjelm, J. 2006, Local positioning systems: LBS Applications and Services, (Boca Raton: Taylor & Francis)

Mendel, J. M. 1995, Lessons in estimation theory for signal processing, communications, and control (New Jersey: Prentice Hall)

Oh, M. K., Park, J. H., & Kim, J. Y. 2009, IR-UWB packet-based precise ranging system for u-home networks, IEEE Trans. Consumer Electronics, 55, 119-125. https://doi.org/10.1109/TCE.2009.4814423

Park, C. S, & Yim, J. G. 2010, A performance comparison of positioning methods considering measurement noise, Journal of Institute of Control, Robotics and Systems, 16, 1176-1181. https://doi.org/10.5302/J.ICROS.2010.16.12.1176

Seong Yun Cho is an assistant professor in the Department of Robot Engineering at Kyungil University. He received B.S., M.S., and Ph.D. degrees from Kwangwoon University. From 2004 to 2013, he worked for the Electronics and Telecommunications Research Institute (ETRI). His research interests include positioning and navigation systems, filtering theory for linear/nonlinear systems, sensors-based motion detection, and LBS application systems.

Dongyeop Kang received his B.S, M.S. and Ph.D. degree from Pohang University of Science and Technology, Korea, in 2006, 2008 and 2013, respectively. He is currently a senior researcher in the Electronics and Telecommunications Research Institute (ETRI). His research interests include control theory, estimation and filtering with applications in robotics and optimization techniques.

Jinhong Kim is a researcher with the Electronics and Telecommunications Research Institute (ETRI). He received B.S. and M.S. degrees from Kyungpook National University. His research interests include indoor localization and navigation, wireless communication, and mobile computing.

Young Jae Lee is a senior engineer in the Daegu-Gyeongbuk research center at ETRI. He received B.S., M.S., and Ph.D. degrees from KAIST. From 2000 to 2004, he worked for Hynix Semiconductor and joined in ETRI from 2004. His research interests are a positioning and navigation systems, IoT connected with the devices, circuit and system design, and logistics.

Ki Young Moon received his BS and MS degrees in electronics engineering in 1986 and 1989, respectively, from Kyungpook National University, Korea. He received the PhD degree in Computer Science from the Chungnam National University, Korea in 2006. He has been a principal member of technical staff in Electronics and Telecommunications Research Institute (ETRI), Korea since 1994 and he is currently working as director of the IT Convergence Research Sector. His research interests include Logistics security, biometrics, distributed system, and application security.

https://doi.org/10.11003/JPNT.2017.6.3.105